Available online at www.sciencedirect.com
SCIENCE DIRECT®
International Journal of Solids and Structures 42 (2005) 1073–1089
INTERNATIONAL JOURNAL OF SOLIDS and STRUCTURES
www.elsevier.com/locate/ijsolstr

On the accuracy of self-consistent elasticity formulations for directionally solidified polycrystal aggregates

Masatsugu Yaguchi [a], Esteban P. Busso [b,*]

[a] *Department of Mechanical Engineering, Imperial College London, Exhibition Road, London SW7 2BX, UK*
[b] *Central Research Institute of the Electric Power Industry, Tokyo, 201-8511, Japan*

Received 2 March 2004; received in revised form 14 July 2004
Available online 18 September 2004

Abstract

In this work, the elastic properties of directionally solidified (DS) polycrystal aggregates are investigated through a combination of analytical and numerical approaches. The effects of crystallographic misorientations and grain aspect ratios of aggregates with ellipsoidal shaped grains are first examined following a self-consistent approach. Finite element techniques are then used to examine the effects of grain size on the elastic properties of the aggregate and to assess the accuracy of the self-consistent predictions. To that purpose, a finite element procedure is presented to generate numerically realistic 3D DS microstructures from electron back-scatter diffraction (EBSD) lattice orientation measurements on an arbitrary cross-section of a DS material. The elastic stiffnesses predicted numerically and analytically are then compared with experimental data on a Ni-base DS alloy tested uniaxially along arbitrary orientations. The general trend predicted analytically was found to be consistent with the numerical and experimental results. Furthermore, an increase in the misorientation between the [0 0 1] axis of each DS grain with respect to the grain growth direction was found to decrease the elastic anisotropy of the DS material.

Keywords: Self-consistent method; Homogenisation; Directionally solidified; Single crystals

1. Introduction

Directionally solidified (DS) polycrystal aggregates are a class of materials with a controlled grain growth direction. By forcing the direction of grain growth to be parallel to that of the maximum principal stress, it is possible to design alloys with greatly improved mechanical properties over similar polycrystals with randomly oriented grain boundaries. DS polycrystals are particularly suitable for high homologous

* Corresponding author. Tel.: +44 20 7594 7084; fax: +44 20 7594 7017.
E-mail addresses: e.busso@imperial.ac.uk, e.busso@ic.ac.uk (E.P. Busso).

0020-7683/$ - see front matter © 2004 Elsevier Ltd. All rights reserved.
doi:10.1016/j.ijsolstr.2004.07.009

temperature applications, such as gas turbine blades and thin films (Williams et al., 2003), since grain boundary diffusion processes weaken the material. Although the macroscopic behaviour of polycrystal aggregates based on single crystal properties has been widely studied (e.g. see Bunge et al., 2000), the behaviour of the DS polycrystals has hardly been addressed. Experimental investigations have been conducted only on a very few DS alloy systems, e.g. Ohno et al. (1992) identified the active slip systems in a DS superalloy and, in Misra et al. (1999), Asthana et al. (2002) and Bei et al. (2003), the effects of microstructure on mechanical properties were determined.

One of the simplest approaches which can be followed to obtain the elastic properties of DS polycrystal aggregates are those based on the Voigt and Reuss averages (e.g. see Hasebe et al., 1992). In the former, it is assumed that the strain in each grain of the aggregate is the same, whereas in the latter uniformity of stress in all grains is considered. Thus, in the Voigt method, the macroscopic elastic stiffness is given as the volume average of the stiffness of all the crystals, an upper bound, and in Reuss's, the macroscopic elastic compliance is defined as the volume average of the compliance of all the crystals, a lower bound for the elastic stiffness of the polycrystal. Even though these methods provide useful bounds for the elastic properties of randomly oriented polycrystals, they are unable to account for some important features of DS materials, such as grain morphology and size, as well as the effects of preferential grain boundary orientations, on the material elastic anisotropy.

Amongst the most successful methods proposed to overcome the limitations of the assumed strain or stress uniformity are those based on mean field approaches, such as the self-consistent method developed from Eshelby's (1957) and Kröner's (1958) work. In this approach, compatibility and equilibrium between grains are satisfied at both the local and the macroscopic levels, hence the term "self-consistent". Furthermore, the interaction between a single crystal grain and its neighbours is treated as that between an ellipsoidal inclusion with the same properties as those of the grain, embedded in an homogeneous equivalent medium which has the same (unknown) properties as those of the macroscopic aggregate. A critical aspect of this method is that the strain distribution within the inclusion is assumed uniform when, in reality, in cases of large property mismatch, it is seldom the case. Kneer (1965) extended Kröner's method to predict the elastic properties of an anisotropic polycrystal, from known single crystal elastic coefficients and lattice orientation distributions. This work was later on applied to polycrystal materials with orthotropic symmetry (Morris, 1970). More recently, Kneer's self-consistent elasticity model was used to predict the elastic properties of DS polycrystals (Hendrix et al., 1998). Here, DS polycrystals of the type shown in Fig. 1(a) were idealised as a uniform array of ellipsoidal grains with a distribution of crystal lattice orientations resulting in a polycrystal with transversely isotropic symmetry along the grain growth direction, as illustrated in Fig. 1(b). Note that, henceforth, the grain growth direction will always be assumed to be parallel

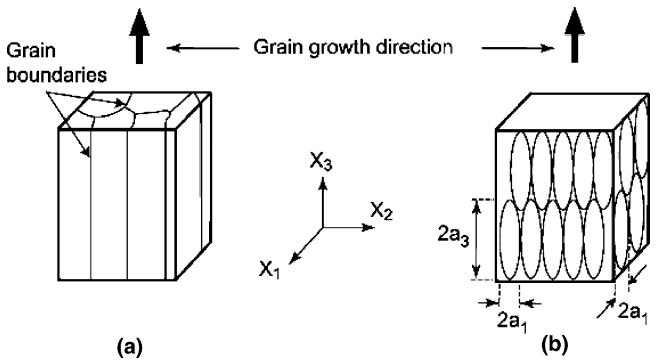

Fig. 1. Schematics of grain morphologies in (a) a directionally solidified polycrystal and (b) an idealized polycrystal aggregate with ellipsoidal grains of dimensions $2a_1 \times 2a_1 \times 2a_3$. Here, the grain growth direction is assumed to be along the X_3 axis.

to the global X_3 reference axis. In the work reported by Hendrix et al. (1998), even though predictions of the elastic behaviour of the transversely isotropic polycrystals were obtained for different crystallographic textures and grain aspect ratios, two important aspects were not addressed. Firstly, the DS microstructure was approximated by that shown in Fig. 1(b), and there was no examination as to the limiting grain aspect ratio above which the ellipsoidal grains could be considered as idealized DS grains. Secondly, the accuracy of the trend predicted by the self-consistent approach was not assessed independently either numerically or experimentally.

In this work, these outstanding issues are addressed. First, the effects of crystallographic misorientations and grain aspect ratios of aggregates of a Ni alloy with ellipsoidal shaped grains are examined following Kneer's (1965) self-consistent approach. Then, the Young's moduli of a Ni base DS polycrystal along different orientations are experimentally measured, and the crystallographic orientations of the DS grains are determined using electron back-scatter diffraction (EBSD) techniques. Finite element analyses of the tested DS specimens are then carried out to examine the effects of grain size on the elastic properties of the DS aggregate and to assess the accuracy of the self-consistent predictions. Finally, the elastic stiffnesses predicted numerically and analytically are then compared with the experimental measurements.

2. Self-consistent formulation

In this section, Kneer's (1965) self-consistent elasticity formulation is summarised. Assuming that the inhomogeneous nature of the microstructure surrounding each grain in a polycrystal can be represented in a statistical sense by a homogeneous matrix having the macroscopic elastic properties of the aggregate, then the stress, $\boldsymbol{\sigma}$, and strain, $\boldsymbol{\epsilon}$, tensors in the single crystal are related to those of the aggregate, namely $\boldsymbol{\sigma}^*$ and $\boldsymbol{\epsilon}^*$, as,

$$\boldsymbol{\epsilon} = (C^{*-1} + U : C^{*-1}) : \boldsymbol{\sigma}^*, \tag{1}$$

$$\boldsymbol{\sigma} = (C^* + C^* : V) : \boldsymbol{\epsilon}^*, \tag{2}$$

where C^* is the elastic stiffness of the aggregate and ':' denotes a double contraction. The fourth order tensors U and V are defined by

$$U = -(C - C^* + C^* : S^{-1})^{-1} : (C - C^*), \tag{3}$$

$$V = (S^{-1} - I) : (C - C^* + C^* : S^{-1})^{-1} : (C - C^*). \tag{4}$$

Here, S is the Eshelby tensor (see Appendix A for its definition) and I is the fourth order unit tensor. The coefficients of the single crystal elastic moduli expressed in a generic global coordinates system, C_{ijkl}, in terms of the independent elastic constants in the lattice coordinates system, c_{mnpq}, are

$$C_{ijkl} = Q_{mi}Q_{nj}Q_{pk}Q_{ql}c_{mnpq}, \tag{5}$$

where Q_{mi} are the components of the rotation matrix

$$\mathbf{Q} = \begin{pmatrix} \cos\psi\cos\phi - \sin\psi\sin\phi\cos\theta & \sin\psi\cos\phi + \cos\psi\sin\phi\cos\theta & \sin\phi\sin\theta \\ -\cos\psi\sin\phi - \sin\psi\cos\phi\cos\theta & -\sin\psi\sin\phi + \cos\psi\cos\phi\cos\theta & \cos\phi\sin\theta \\ \sin\psi\sin\theta & -\cos\psi\sin\theta & \cos\theta \end{pmatrix}. \tag{6}$$

The Euler angles (ψ, θ, ϕ) in Eq. (6) are defined so that they map the global coordinate system (X_1, X_2, X_3) into the cubic crystallographic axes, see Fig. 2(b).

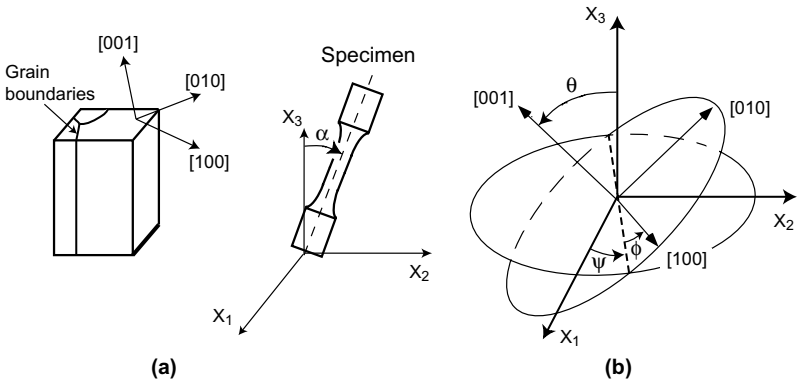

Fig. 2. Definition of (a) the angle between the grain growth direction and the specimen axis, α, and (b) the Euler angles, (ψ, θ, ϕ), between the crystallographic axes of each grain and the global axes.

From Eqs. (1) and (2), two different self-consistent conditions can be defined. The first condition yields a value of C^{*-1} which makes the average deviation of U of each grain from that of the aggregate, viz., $\langle U \rangle$, to be zero. It can be shown that such condition implies that the average strain in all the grains, $\langle \boldsymbol{\epsilon} \rangle$, equals the overall DS aggregate strain, i.e. $\langle \boldsymbol{\epsilon} \rangle = \boldsymbol{\epsilon}^*$. The second condition gives a value of C^* which makes the average deviation of the value of V for each grain from that of the aggregate, $\langle V \rangle$, to be zero. This implies that the average stress in the grains, $\langle \boldsymbol{\sigma} \rangle$, must be equal to the overall aggregate stress, i.e. $\langle \boldsymbol{\sigma} \rangle = \boldsymbol{\sigma}^*$. It can also be shown (e.g. see Hendrix et al., 1998) that $\langle U \rangle$ and $\langle V \rangle$ become zero with the same value of C^*.

Since the Eshelby tensor, S, is a function of C^*, then the value of C^* which satisfies the $\langle U \rangle = \langle V \rangle = 0$ condition cannot be calculated explicitly, and an iterative procedure is needed to determine it. In this work, the first guess, $C^{*(1)}$, is taken to be the mean value of the Voigt and Reuss bounds. In any subsequent iteration (r), C^* is approximated by

$$C^{*(r+1)} = C^{*(r)} - \Delta C^{*(r)} \tag{7}$$

and successive values are taken until convergence is achieved. The ΔC^* corrections in Eq. (7) are calculated from the expressions given in Eqs. (3) and (4) (Morris, 1970; Hendrix et al., 1998)

$$\Delta C^* = C^* : S^{-1} : \langle U \rangle, \tag{8}$$

$$\Delta C^* = C^* : [S : (I - S^{-1})]^{-1} : \langle V \rangle. \tag{9}$$

Here, $\langle U \rangle$ and $\langle V \rangle$ are taken over all crystal orientations according to the frequency of occurrence as follows,

$$\langle U \rangle = \int_0^{2\pi} \int_0^{\pi} \int_0^{2\pi} \omega U \sin\theta \, \mathrm{d}\psi \, \mathrm{d}\theta \, \mathrm{d}\phi, \qquad \langle V \rangle = \int_0^{2\pi} \int_0^{\pi} \int_0^{2\pi} \omega V \sin\theta \, \mathrm{d}\psi \, \mathrm{d}\theta \, \mathrm{d}\phi, \tag{10}$$

where ω is the crystallite orientation distribution function.

3. Experimental procedures

In this section, the experimental procedures to measure the anisotropic Young's moduli and the transgranular and intergranular misorientations in a typical DS polycrystal using EBSD techniques are given.

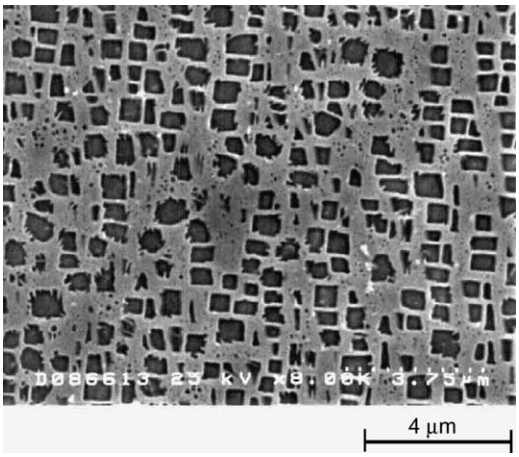

Fig. 3. SEM micrograph of a typical directionally solidified superalloy microstructure showing the Ni_3Al precipitates.

Fig. 3 shows an SEM micrograph of a typical Ni base DS superalloy widely used in gas turbine blade applications. It consists of cuboidal Ni_3Al precipitates (γ'), with an ordered FCC or $L1_2$ structure, distributed in a Ni solid solution FCC matrix (γ). The volume fraction of the 0.5–1.0 μm size precipitates is 26%. Furthermore, the transversal size of the grains—that is in a direction perpendicular to the grain growth direction—ranges from 200 to 5000 μm. It should also be noted that, generally, the [0 0 1] crystallographic orientation of each grain does not coincide with the growth direction of the DS alloy, as it will be discussed later on.

Since there was no elastic stiffness data available for the individual single crystal grains of the DS alloy, the elastic moduli of each grain was estimated from the elastic coefficients of the individual single crystal phases using the Voigt and Reuss bounds and data from Pollock and Argon (1994). Table 1 shows the estimated stiffness coefficients for the superalloy single crystal at 870 °C. Note that the small differences between the Voigt and Reuss bounds are due to fact that the elastic stiffnesses of the individual phases are very similar. Since these values are in fact upper and lower bounds, there was no need for obtaining self-consistent estimates. Thus, the average values of the two bounds will be considered to be representative of those of the individual two-phase grains in the DS alloy. No effect of the precipitate size distribution on the elastic behaviour of each single crystal grain was included since the effect of precipitate size on the mechanical properties of superalloy single crystals has been shown to be negligible when the precipitate volume fraction is below ~50% (e.g., see Busso et al., 2000; Meissonnier et al., 2001).

Fig. 4 shows the dimensions of the uniaxial test specimen used to measure the DS alloy Young's modulus at different orientations. The test specimens were machined from DS superalloy plates so that the angle between the grain growth direction and the axis of the specimen, e.g. α in Fig. 2(a), was 0°, 30°, 45°, 60° and

Table 1
Elastic stiffness coefficients (in GPa) of the individual single crystal grains of the DS material at 870 °C

	C_{11}	C_{12}	C_{44}
γ(FCC)	208.0	142.0	100.0
$\gamma'(L1_2)$	184.0	124.0	94.0
Voigt	201.8	137.4	98.5
Reuss	201.2	136.8	98.4
Average	201.5	137.1	98.5

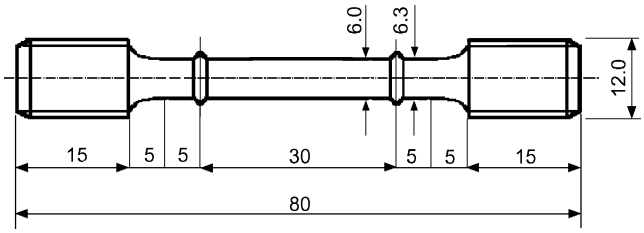

Fig. 4. Test specimen geometry (all dimensions in mm).

90°. For each orientation, three test specimens were machined from different DS plates to account for statistical differences in grain boundary distributions and DS grain lattice orientations. Tensile tests were then conducted on these specimens at 870 °C and constant strain rates of 10^{-6} and 10^{-3} s^{-1} using a servo-hydraulic testing machine and a radiant furnace. Young's modulus were measured from the resulting stress–strain curves. The actual test results will be presented in Section 5, when discussing the relative accuracy of the analytical and numerical predictions.

EBSD measurements on tested specimens were conducted to investigate the transgranular and intergranular misorientations of the DS material. An EBSD sample of an undeformed material was cut out from the shoulder of a test specimen with an orientation angle of $\alpha = 45°$. Furthermore, the orientation of the analysed surface was perpendicular to the specimen axis.

Fig. 5 shows the EBSD measured high-angle grain boundaries on the undeformed sample cross section. White lines define neighbouring regions which are misoriented by more than 15°, and black lines regions where the misorientations are between 5° and 15°. Thus, the former can be considered to be high-angle grain boundaries and the latter sub-grain boundaries. These EBSD results also reveal that there is a wide range of grain sizes in the polycrystal, and that sub-grain boundaries are present in both small and large grains.

The corresponding distribution of the specimen loading axis onto the lattice of each crystal is shown in Fig. 6's standard stereographic triangle. Here, the gray scale contrast of each point corresponds to that

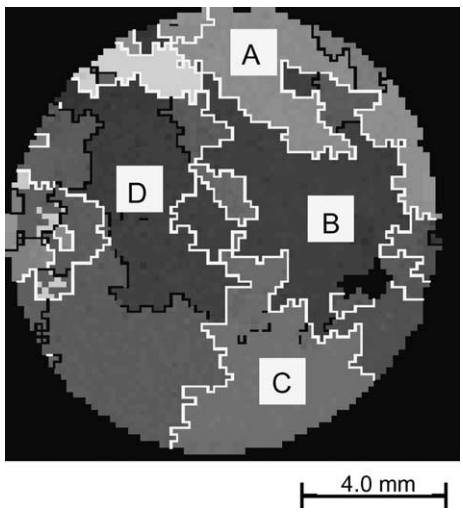

Fig. 5. Grain boundaries identification based on the EBSD measurements on the shoulder of a specimen whose axis is at 45° from the grain growth direction.

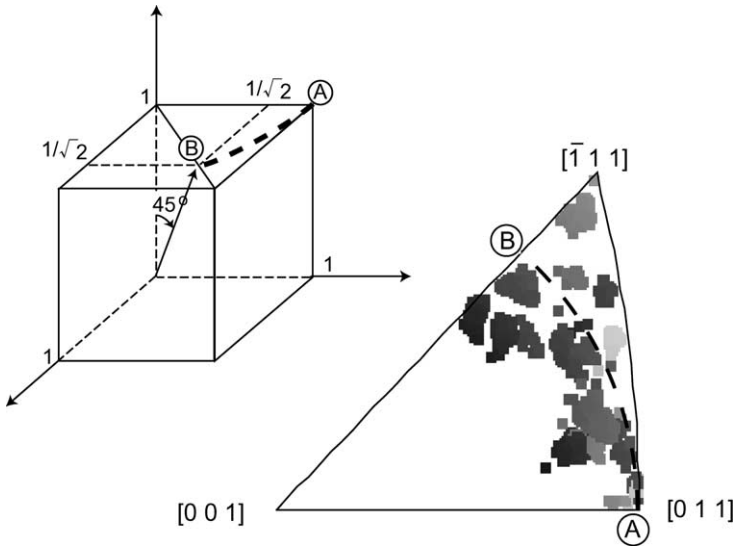

Fig. 6. Loading axis in the standard stereographic triangle.

shown in Fig. 5's EBSD orientation map. It is worth noting that if the [0 0 1] lattice orientation at each point in the cross-section was perfectly aligned with the DS material's grain growth direction ($\theta = 0$ in Fig. 2(b)), then all data points in Fig. 6 would fall on a perfect arc passing through the [0 1 1] vertex of the stereographic triangle (given by the dashed line between A and B in Fig. 6), as the misorientation angle (α) of the specimen is always equal to 45°. The fact that there are points at either side of the line as well implies that the [0 0 1] axes of the grains do not always coincide with the grain growth direction.

Fig. 7 shows the distributions of the Euler angles measured in Fig. 5's cross-section. Fig. 7(a) gives the distributions of the angle θ, and Fig. 7(b) those of the angles ψ and ϕ. The solid line in Fig. 7(a) represents the fitting to the data using a Gaussian distribution. The measured variation of the angle θ is $-3.8° \pm 10°$. The labels A, B, C and D in Fig. 7(b) identify the orientations of Fig. 5's grains. It can also be seen that

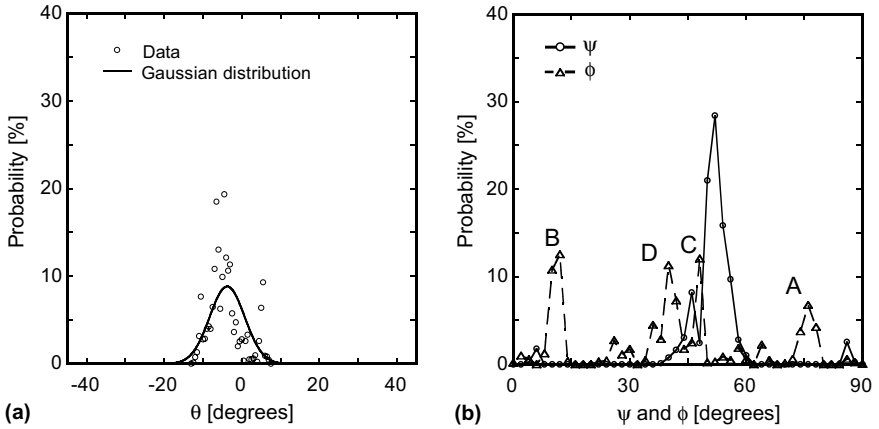

Fig. 7. Distribution of the EBSD measured Euler angles on the cross-section of Fig. 4's specimen: (a) θ, and (b) ψ and ϕ.

intergranular variations of the Euler angle ϕ are present. The results also show that transgranular misorientation distributions within each grain do not exceed 10°.

4. FE procedure to generate DS microstructures

In this section, the FE procedure to generate three-dimensional (3D) DS microstructures will be described. The general approach relies on an extrapolation of the lattice orientations measured by EBSD on an arbitrary cross-section onto the individual integration points of the 3D FE mesh of the DS specimen of interest.

The general principle behind the extrapolation procedure is illustrated in Fig. 8. Here, it is assumed that (i) the lattice orientation of each DS grain remains unchanged along the grain growth direction, viz. X_3 axis in Fig. 8(a), and that (ii) points with global (X_1, X_2) coordinates have the same orientations as those with the same (X_1, X_2) coordinates on the plane on which the EBSD measurements were carried out. Assume for simplicity that that the reference EBSD plane is normal to the direction of grain growth in the DS alloy (see Fig. 8(a)). The first step in the procedure consists of assigning the orientations measured on this X_3 plane onto a plane normal to the axis of the specimen, which is oriented at an angle α with respect to the X_3 axis. Thus, the orientation of a generic point on the specimen's reference X'_3 plane, of coordinates $(X'_1, X_{20}/\cos\alpha, 0)$ are assigned to be that of its corresponding point on the X_3 plane, of coordinates (X_1, X_{20}, X_3) (see Fig. 8(a)). In the second and final step, the lattice orientation of a generic material point of local coordinates (X'^P_1, X'^P_2, X'^P_3) is assigned to be that of its image point in the reference $X'_3 = 0$ plane defined in the previous step (see Fig. 8(b)). Thus, the orientation of this generic material point P in the specimen will be the same as that of its image point in the specimen's local $X'_3 = 0$ reference plane of coordinates $(X'^P_1, X'^P_2 + X'^P_3 \tan\alpha, 0)$ (see Fig. 8(b)). Note that when the EBSD measurements were made on an area not large enough to enable the lattice orientations to be extrapolated to the whole specimen, the EBSD data was reproduced periodically.

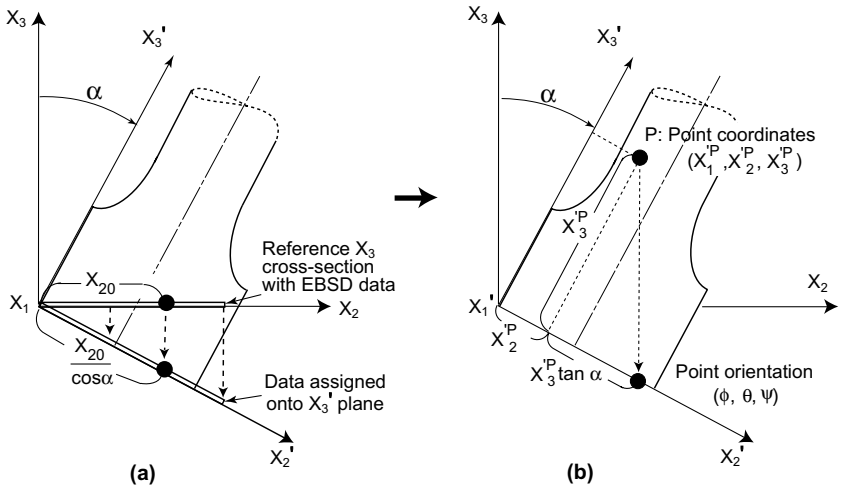

Fig. 8. Schematics of how lattice orientations are extrapolated to the material points of a specimen with an arbitrary misorientation angle (α) based on the orientations of a reference cross-section measured by EBSD: (a) extrapolation of the X_3 reference plane data onto a local X'_3-plane, and (b) assignment of the orientation of a generic point P in the specimen with the angle α.

The FE analyses were conducted on the tensile test specimen shown in Fig. 4 to calculate the DS material Young's modulus along different orientations using a commercial FE code and (ABAQUS, 2001). A typical FE mesh consisted of 2000 quadratic elements with reduced integration. Appropriate boundary conditions were imposed at the specimen's ends to simulate the gripping action on the specimen during the test. Specimens with misorientation angles (α) of 0°, 30°, 45°, 60° and 90° were tested.

In addition to the EBSD based DS microstructures generated as described above, DS polycrystals were generated numerically to examine the effect of grain size on Young's modulus. Square cross-section polycrystal bars containing four square DS grains of either 1 mm (*Small*) or 3 mm (*Large*) in size were considered. The orientation of each grain was assumed to be given by those of grains A, B, C and D in Fig. 5. The distribution of the Euler angles within each grain was generated using Gaussian random numbers, and the method of assigning the Euler angles to the polycrystal material points was the same as that described above. The misorientation angles (α) for these bars were 0°, 30°, 45°, 60°, 75°, 85° and 90°.

5. Results and discussions

In this section, the predicted elastic stiffnesses of the idealized ellipsoidal grain polycrystals obtained from the self-consistent elasticity formulation are shown as functions of the aspect ratio and the grain growth direction—[0 0 1] lattice angle, viz. θ in Fig. 2(b). The predicted Young's moduli for the actual DS superalloy are then compared with the experimental and FE results to assess the relative accuracy and range of validity of the analytical solutions.

In DS superalloys, only the crystallographic orientation of each grain parallel to the grain growth direction can be controlled to lie within a certain band, whereas the transverse orientation of each grain is fully random. In the experimental elastic and EBSD data and the FE predictions of the uniaxial specimen behaviour, the ratio between the size of the representative volume element of interest to the mean transversal grain size is relatively small (i.e. small numbers of grains in the material volume). Thus the transverse orientations of just a few grains determine the distributions of the Euler angles ψ and ϕ of the aggregate. This is the case shown in Fig. 7(b) due to the small number of grains found in the specimen cross-section (e.g. see Fig. 5). The self-consistent formulation, on the other hand, describes the elastic behaviour of a representative volume element of a DS material whose size is much greater than the mean transversal grain size. In the limit, when the distribution of the transversal orientations of the aggregate is determined by an infinitely large number of grains, one can safely assumed that the resulting distribution will be uniform. Thus the crystallite orientation distribution function ω in Eq. (10) is assumed to give uniform distributions with regards to the Euler angles ψ and ϕ (i.e., $\omega = \text{constant} = 1/2\pi$, for both ψ and ϕ).

Henceforth, Voigt two-index notation for transversely isotropic materials will be used to express the elastic stiffness coefficients, viz. $C_{11} = C_{1111} = C_{2222}$, $C_{33} = C_{3333}$, $C_{12} = C_{1122}$, $C_{13} = C_{1133} = C_{2233}$, $C_{44} = C_{2323} = C_{3131}$, and $C_{66} = C_{1212}$.

5.1. Self-consistent predictions of the elastic moduli

5.1.1. Elastic stiffness coefficients

Fig. 9 shows the self-consistent predictions of the stiffness coefficients as a function of the grain aspect ratio, a_3/a_1, for a perfectly [0 0 1] oriented ellipsoidal grained polycrystal, that is when $\theta = 0$ in Fig. 2(b). As $2a_1$ and $2a_3$ depict the size of the ellipsoidal grain in a direction perpendicular and parallel to the grain growth direction, respectively, an increase in the grain aspect ratio implies an elongation of the grain along the grain growth direction. In these results, the stiffness coefficients C_{11}, C_{12} and C_{66} can be seen to depend on the grain aspect ratio, while C_{33},C_{13} and C_{44} do not. By increasing the grain aspect ratio from 0.01 to 100, C_{11} and C_{66} decrease and C_{12} increases, and their variations saturate for aspect ratios above 100 or

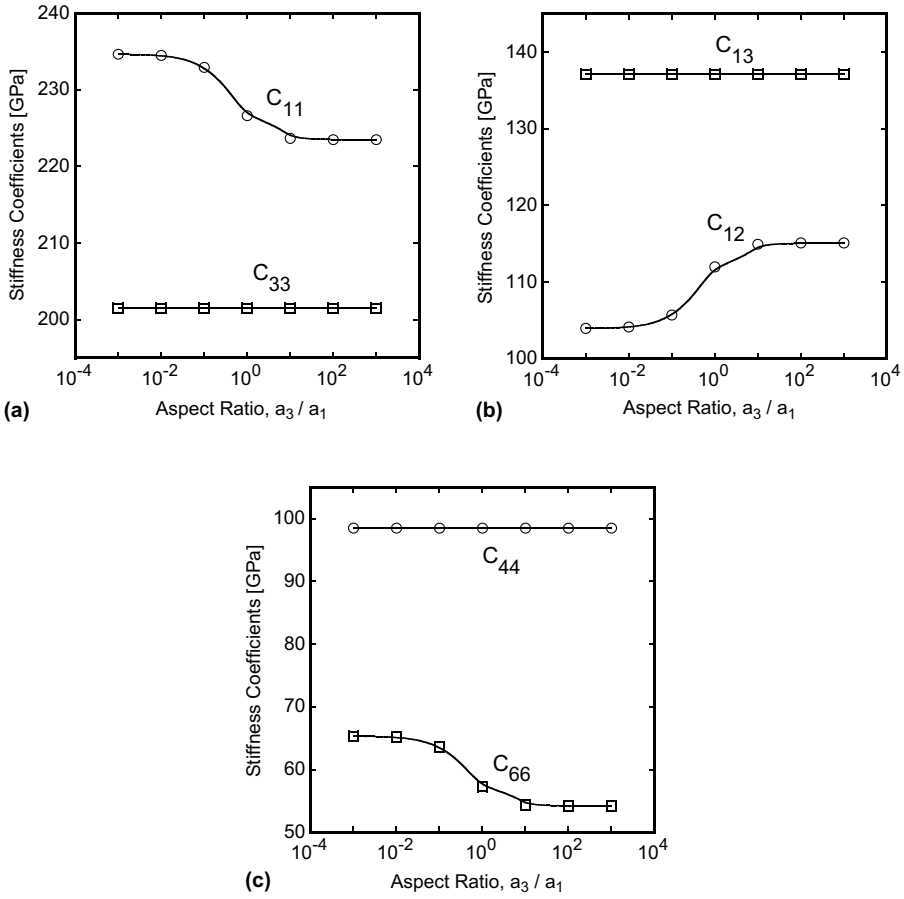

Fig. 9. Self-consistent predictions of the stiffness coefficients for a perfectly [0 0 1] oriented ellipsoidal grained polycrystal as a function of the grains' aspect ratio: (a) C_{11} and C_{33}, (b) C_{12} and C_{13}, and (c) C_{44} and C_{66}.

below 0.01. Since a perfect DS polycrystal such as that illustrated in Fig. 1(a) could, as a first approximation, be modelled as an ellipsoidal grained polycrystal when $a_3/a_1 \to \infty$, these results suggest that ellipsoidal grain polycrystals with aspect ratios greater than $a_3/a_1 > 100$ should be the best approximation to the elastic behaviour of a DS material.

The predicted stiffness coefficients for an ellipsoidal grained polycrystal where the [0 0 1] axis of each grain does not coincide with the grain growth direction, i.e. $\theta \neq 0$ in Fig. 2(b), are shown in Fig. 10. The effect of the misorientation angle θ on the stiffness coefficients for $a_3/a_1 = 1$ is shown in Fig. 10(a). Note that the angle θ is assumed to be the same in every grain. Although all the stiffness coefficients vary with the angle θ, C_{33}, C_{13} and C_{44} exhibit the largest dependency. It should also be pointed out that when the angle θ is equal to 32°, there are only three independent elastic constants, namely C_{11} ($=C_{33}$), C_{12} ($=C_{13}$), and C_{44} ($=C_{66}$), which corresponds to an anisotropy factor, $2C_{44}/(C_{11} - C_{12})$, equal to 1. This implies that the DS material with this orientation is elastically isotropic. The anisotropy factor for the individual single crystal grains of the DS alloy under study is 3.06. The effect of the grain aspect ratio on the stiffness coefficients of an ellipsoidal grained polycrystal with a misorientation angle of $\theta = 20°$ is shown in Fig. 10(b). It can be seen that the effect of the grain aspect ratio on the stiffness coefficients is non-zero but rather negligible.

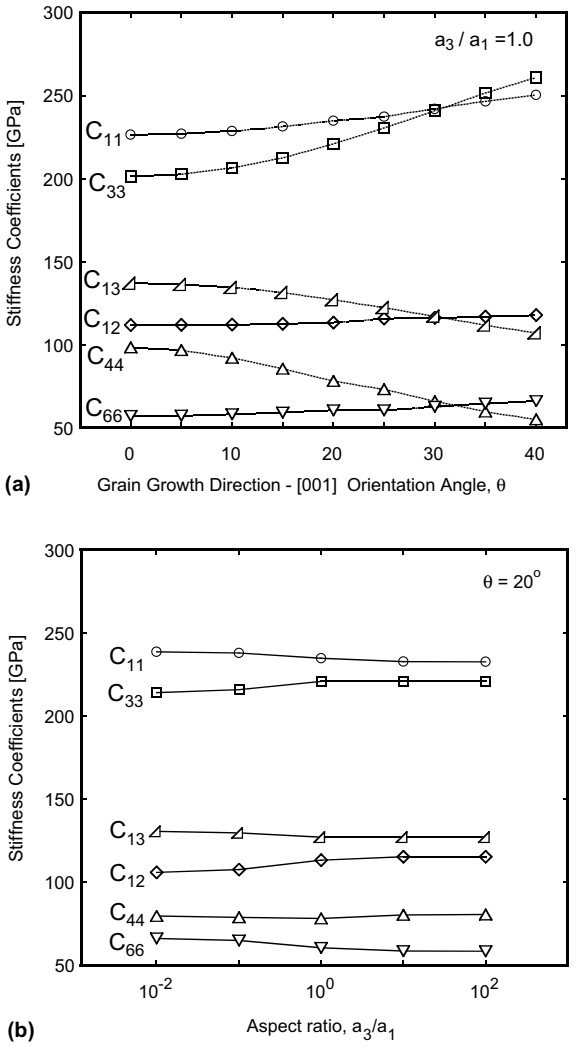

Fig. 10. Self-consistent predictions of the stiffness coefficients for a misoriented ellipsoidal grained polycrystal: (a) effect of the angle between the grain growth direction and the [0 0 1] axis, θ, for grains with an aspect ratio of $a_3/a_1 = 1$, and (b) effect of the grain aspect ratio on a polycrystal with uniform orientation of $\theta = 20°$.

5.1.2. *Effect of specimen axis—grain growth direction angle*

Fig. 11 shows the predicted effect of the angle between the grain growth direction and the specimen axis, α in Fig. 2(a), on the elastic modulus of a perfectly [0 0 1] oriented ellipsoidal grained polycrystal with different grain aspect ratios. Here, the elastic modulus along the relative orientation defined by the angle α is given by the inverse of the elastic compliance coefficient in the local (X'_1, X'_2, X'_3) system, S'_{33}. It can be seen that the elastic modulus depends strongly on the angle α, and weakly on the grain aspect ratio. The more compliant orientation corresponds to $\alpha = 0°$, which is equal to the [0 0 1] modulus, E_{001}, and the elastic modulus increases rapidly with the angle α till it reaches 50°. At this point, the Young's modulus is more than double its value at $\alpha = 0°$. For $\alpha > 50°$, it then decreases rapidly and its sensitivity to the grain aspect ratio becomes most pronounced. The ellipsoidal grain aspect ratio also has an effect on the Young's moduli

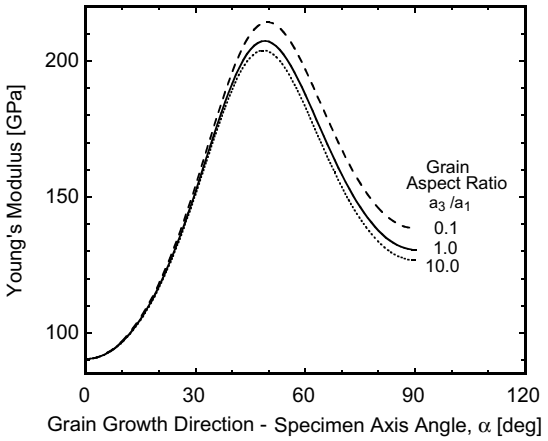

Fig. 11. Effect of the angle between the grain growth direction and the specimen axis, α, on the predicted Young's modulus of a polycrystal with ellipsoidal grains of different aspect ratios (a_3/a_1) and with their [0 0 1] axis aligned with the grain growth direction (i.e. $\theta = 0$ in Fig. 2(b)).

of the perfectly oriented polycrystal, in particular when the angle α is larger than 40°. For larger grain aspect ratios, the elastic stiffness along the direction defined by α decreases. In such cases, that is for needle shaped grains aligned along the grain growth direction, i.e. X_3 in Fig. 2(a), the transversal boundary conditions imposed on the grains by their surroundings behave more like the uniform stress condition of the Reuss model (Hasebe et al., 1992). In contrast, grains with small grain aspect ratios experience in-plane conditions closer to the uniform strain assumptions prevailing in Voigt-type models. When the angle α is less than 30°, the effect of the aspect ratio on Young's moduli is found to be negligible. This predicted trend is consistent since no grain aspect ratio effect is expected on the Young's moduli of constituent grains along the X_3 direction when the [0 0 1] crystallographic axis of each grain is perfectly oriented with the grain growth direction (e.g. $\alpha = 0°$ in Fig. 11).

Fig. 12 shows the effect of the angle α on the Young's modulus of ellipsoidal grained polycrystals with (a) different angles between the grain growth direction and the [0 0 1] axis of each grain, θ, and $a_3/a_1 = 100$, and with (b) different grain aspect ratios (a_3/a_1) and $\theta = 20°$. As Fig. 12(a) reveals, when θ increases, the Young's moduli for angles around $\alpha = 0°$ and $\alpha = 90°$ increase, while decreasing in the region around $\alpha = 50°$. Thus, by tilting the [0 0 1] axis of each grain away from the grain growth direction (X_3-axis), the level of elastic anisotropy of the aggregate decreases since the variation of its uniaxial stiffness with the angle α decreases.

In Fig. 12(b), the effect of the grain aspect ratio for the misoriented material with $\alpha \geqslant 40°$ is similar to that of the perfectly [0 0 1] oriented material case ($\theta = 0°$) discussed in Fig. 11, namely the larger the grain aspect ratio, the lower the Young's modulus of the aggregate is. However, a different trend was found for the stiffness along directions defined by angles $\alpha < 40°$. Here, aggregates with grain aspect ratios lower than one are predicted to be more compliant than $a_3/a_1 \geqslant 1.0$. However, it should be kept in mind that this effect decreases with a decrease of the lattice misorientation angle θ, and disappears completely for aggregates with perfectly oriented grains ($\theta = 0$), as shown in Fig. 11. This is due to the fact that, when the lattice misorientation angle $\theta \neq 0$, there exists some inhomogeneity of Young's modulus along the X_3 direction among the individual constituent grains. This additional effect of grain aspect ratio can also be interpreted as follows. When $a_3/a_1 = 0.01$, grains will be needle-like in shape lying in the $X_1 - X_2$ plane. Thus, the polycrystal stiffness for the $\alpha = 0$ case will be a lower bound, consistent with the quasi-uniform stress conditions experienced by the grains (i.e. Reuss). When $\alpha = 90°$, one would expect an upper bound stiffness due to the uniform strain conditions seen by the polycrystal (i.e. Voigt).

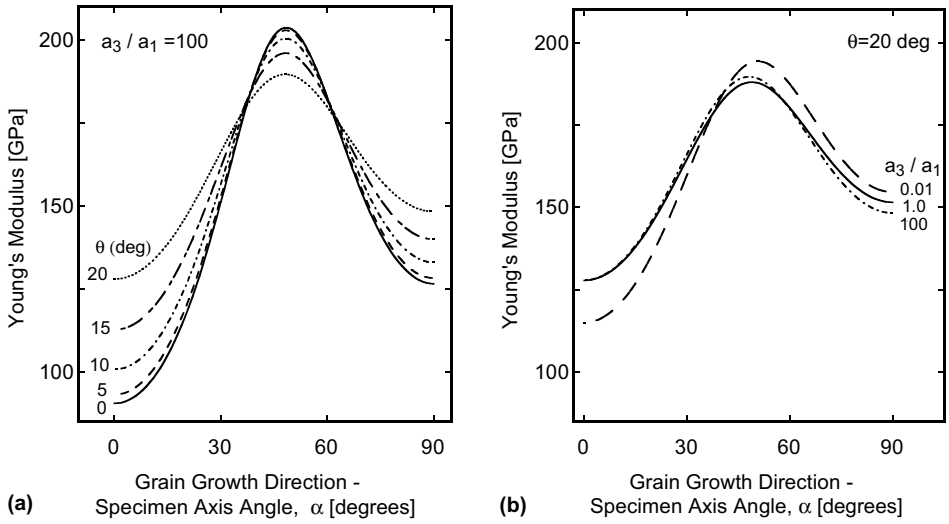

Fig. 12. Predicted effect of the angle between the grain growth direction and the specimen axis, α, on the Young's modulus of ellipsoidal grained polycrystals with (a) different angles between the grain growth direction and the [0 0 1] axis of each grain, θ, and $a_3/a_1 = 100$, and with (b) different grain aspect ratios (a_3/a_1) and $\theta = 20°$.

5.2. Experimental validation of self-consistent approach

A comparison between the self-consistent predictions with experimentally measured Young's modulus obtained from monotonic tensile tests on the Ni-base DS superalloy described in Section 2 is given in Fig. 13. In the self-consistent calculations, the crystallite orientation distribution function for the Euler angles θ was assumed to be given by a Gaussian distribution and fitted to the EBSD data (see Fig. 7(a)).

The experimentally measured DS material stiffnesses along the orientation defined by the grain growth direction - specimen axis angle α exhibit a similar trend to the predicted ones with $a_3/a_1 = 1.0$ and 100. The minimum measured value is also found at $\alpha = 0°$, and the material stiffness increases with the angle, up to $\alpha = 60°$. A general decrease in the stiffness is then seen for $\alpha > 60°$. Note that the relatively large scatter of the data is likely to be due the small number of grains in the gauge section of each test specimen, as can be seen in Fig. 5. Also shown in Fig. 13 are the FE results which will be discussed in the next section. The predictions with a grain aspect ratio of 100 are regarded as more appropriate to describe the actual grain morphology of the DS material. Nevertheless, the predicted grain aspect ratio effect is seen mostly when $\alpha > 40°$, yielding a stiffer response for the smaller grain aspect ratio, as shown previously in Fig. 11. The validity of this effect will be discussed in the next section.

5.3. Validation of the self-consistent approach through FE analyses

With the DS microstructures generated by the procedure discussed in Section 4, FE analyses were conducted on test specimens with different angles α to ascertain the elastic response of the DS polycrystal numerically. Fig. 14 shows typical FE contour plots of the axial stress and strain distributions in a 3D DS specimen whose axis is at 45° with respect to the grain growth direction. It can be seen that the patterns of both the axial strain and stress are aligned with the 45° grain boundaries in the specimen gauge length.

Young's moduli were obtained from the corresponding average stress-strain responses of the specimens' gauge lengths. The resulting predicted Young's modulus are shown in Fig. 13—labelled "FE results with

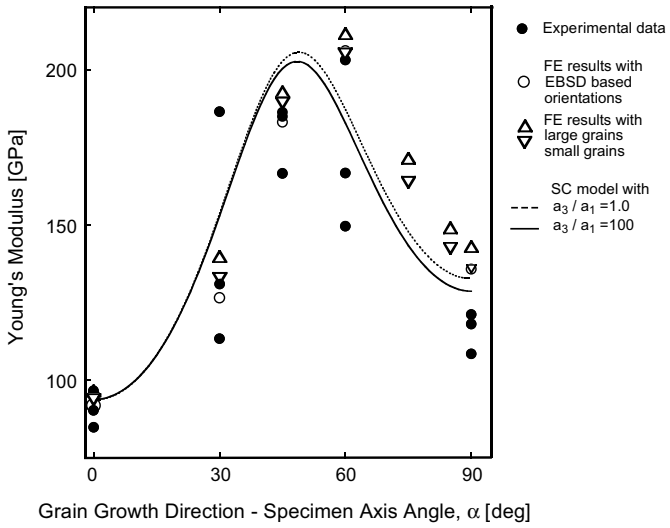

Fig. 13. Comparison between the experimentally measured Young's modulus for the DS alloy along different grain growth direction—specimen axis angle, α, and the analytical (SC) and numerical (FE) predictions.

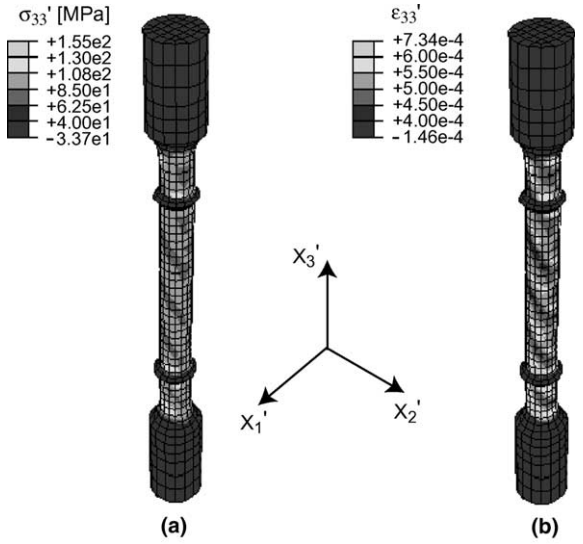

Fig. 14. Predicted distributions of (a) axial stress and (b) axial strain in a 3D FE model of a DS specimen aligned at 45° with respect to the grain growth direction and with orientations extrapolated from the EBSD measurements following the methodology described in Section 4 (see also Fig. 8).

EBSD based orientations''. When the FE predictions are compared with the experimental data, an adequate agreement in the overall trend is found. The FE predictions overestimate the experimentally measured stiffness for $\alpha = 60°$ and 90°, but are within the scatter of the data for smaller angles. A comparison between the FE and the self-consistent predictions also revealed a reasonable agreement between the overall trends, with the latter overpredicting the stiffness for $\alpha < 50°$, and underpredicting it for $\alpha \geqslant 50°$.

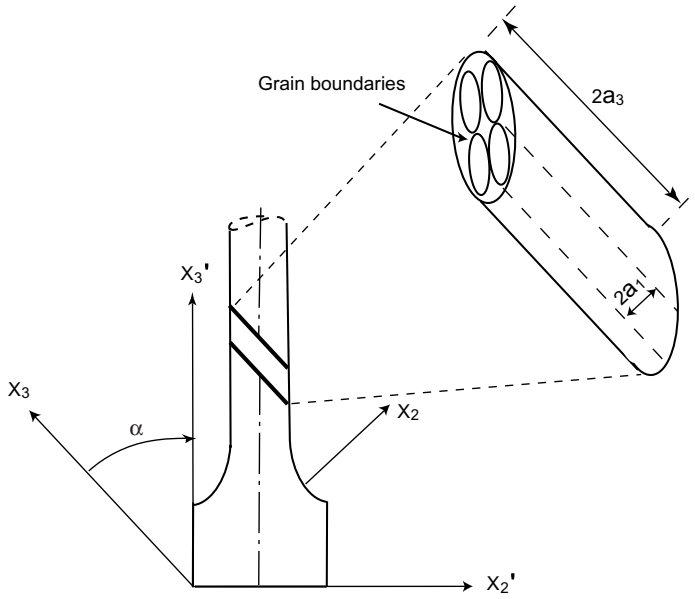

Fig. 15. Link between the transversal dimension of each grain ($2a_1$) with its aspect ratio (a_3/a_1) in DS polycrystal specimens.

The effect of grain size on Young's moduli was investigated by calculating the numerical response of 3D representative volume elements (RVE) of the aggregates containing cuboidal shaped grains of different sizes, as discussed in Section 4. The motivation for the RVE study was based on morphological considerations of the DS specimen microstructure, as illustrated in Fig. 15. Since the axial dimension of the grains ($2a_3$) in misoriented specimens ($\alpha > 0$) is limited by the gauge length surfaces, DS specimens with small grain sizes ($2a_1$) tend also to be associated with large a_3/a_1 ratios, and viceversa for specimens with large grain sizes. Thus a separate study of RVEs of the DS microstructure with similar morphological characteristics should reveal the effects of grain size and grain aspect ratio. The results of the RVE calculations are given in Fig. 13 by the triangular open symbols for two different grain sizes, namely 1 mm size grains (*small*) and 3 mm size grains (*large*). It can be seen that the smaller the grain size, the lower the Young's modulus is for any angle except $\alpha = 0°$. Based on these results, the grain size trend predicted by the FE results in Fig. 13 is consistent with the aspect ratio trend predicted by the self-consistent approach, lending validity to the latter approach.

It should be pointed out that one inherent limitation of the self-consistent approach followed in this study is the fact that there is no explicit account of the effects of grain size distributions, as grain size *per se* is not an explicit variable in the formulation. Furthermore, as in the self-consistent framework each grain is assumed to be embedded in a homogeneous medium, misorientation effects between neighboring grains cannot be considered. However, the 3D FE model of the uniaxial specimens discussed in this work did incorporate explicitly both grain size and transgranular and intergranular misorientations through the extrapolated EBSD measurements. The results summarised in Fig. 13 show that, despite these limitations, the trend predicted by the self-consistent model is consistent with that predicted by the FE results.

6. Conclusions

A self-consistent elasticity formulation for anisotropic polycrystals was applied to study the elastic anisotropy of directionally solidified (DS) materials. To that purpose, the DS polycrystals were idealized

as ellipsoidal polycrystals. An examination of the effects of grain aspect ratio and grain misorientation on the elastic stiffness revealed that the grain aspect ratio becomes saturated with increasingly elongated grains along the grain growth direction, and that an increase in the misorientation of the [0 0 1] crystallographic axis of each grain with respect to the grain growth direction leads to a decrease in the overall anisotropy of the material. The applicability of the self-consistent predictions to an actual DS polycrystal was assessed on a Ni base DS superalloy. Actual EBSD measured lattice orientations were used in the self-consistent calculations and the resulting elastic stiffness predictions along different orientations of the DS alloy with respect to the grain growth direction were found to be consistent with both the experimental trend and the FE predictions of the 3D DS test specimen. The effects of grain size on the material stiffness determined through FE calculations of representative volume elements of the DS alloy were found to be within 5% for orientations away from the grain growth directions.

Acknowledgment

This work was performed when MY was at Imperial College London on leave from the Central Research Institute of the Electric Power Industry (CRIEPI) of Japan. Financial support by CRIEPI is gratefully acknowledged. ABAQUS was provided under academic license by HKS Inc., Providence, Rhode Island, USA.

Appendix A

The Eshelby tensor was numerically calculated following Mura's (1982) work. Its coefficients are defined as

$$S_{ijmn} = \frac{1}{4}(\Gamma_{ikjl} + \Gamma_{iljk} + \Gamma_{jkil} + \Gamma_{jlik})C^*_{klmn}, \tag{A.1}$$

$$\Gamma_{ikjl} = \frac{1}{4\pi}\int_0^{\pi}\int_0^{2\pi} \gamma_{ikjl}\sin\Phi_2\,\mathrm{d}\Phi_1\,\mathrm{d}\Phi_2, \tag{A.2}$$

$$\gamma_{ikjl} = K^{-1}_{ik}(\xi)\xi_j\xi_l, \tag{A.3}$$

where

$$K_{ip}(\xi) = C^*_{ijpl}\xi_j\xi_l, \tag{A.4}$$

and

$$\xi_1 = \frac{\cos\Phi_1\sin\Phi_2}{a_1}, \tag{A.5}$$

$$\xi_2 = \frac{\sin\Phi_1\sin\Phi_2}{a_1}, \tag{A.6}$$

$$\xi_3 = \frac{\cos\Phi_2}{a_3}. \tag{A.7}$$

Here, $0 < \Phi_1 < 2\pi$ and $0 < \Phi_2 < \pi$, are the spherical coordinates that define the direction of the vector $\boldsymbol{\xi}$ with respect to the principal axes of the ellipsoid, of length $2a_1 \times 2a_1 \times 2a_3$.

References

ABAQUS, 2001. Version 6.2. HKS Inc., Providence, Rhode Island.
Asthana, R., Tiwari, R., Tewari, S.N., 2002. Mater. Sci. Eng. A336, 99.
Bei, H., George, E.P., Kenik, E.A., Pharr, G.M., 2003. Acta Mater. 51, 6241.
Bunge, H.J., Kiewel, R., Reinert, Th., Fritsche, L., 2000. J. Mech. Phys. Solids 48, 29.
Busso, E.P., Meissonnier, F., O'Dowd, N.P., 2000. J. Mech. Phys. Solids 48, 2333–2361.
Eshelby, J.D., 1957. Proc. R. Soc. Lond. A241, 376.
Hasebe, T., Sakane, M., Ohnami, M., 1992. J. Eng. Mater. Tech. 114, 141.
Hendrix, B.C., Yu, L.G., 1998. Acta Mater. 46, 127.
Kneer, G., 1965. Phys. Stat. Sol. 9, 825.
Kröner, E., 1958. Z. Phys. 151, 504.
Meissonnier, F., Busso, E.P., O'Dowd, N.P., 2001. Int. J. Plasticity 17 (4), 601–640.
Misra, A., Gibala, R., Noebe, R.D., 1999. Metall. Mater. Trans. 30A, 1003.
Morris, P.R., 1970. Int. J. Engng. Sci. 8, 49.
Mura, T., 1982. Miromechanics of Defects in Solids, Martinus Nijhoff (publ.).
Ohno, N., Mizuno, T., Kawaji, H., Okada, I., 1992. Acta Metall. Mater. 40, 559.
Pollock, T.M., Argon, A.S., 1994. Acta Metall. Mater. 42 (17), 1859.
Williams, J.C., Starke Jr., E.A., 2003. Acta Mater. 51, 5775.